A probability tomography approach to the analysis of potential field data in the Campi Flegrei caldera (Italy)

Teresa Iuliano ([1]), **Paolo Mauriello** ([2]) and **Domenico Patella** ([1])
(1) *Dipartimento di Scienze Fisiche, Università «Federico II», Napoli, Italy*
(2) *Istituto per le Tecnologie Applicate ai Beni Culturali, CNR, Roma, Italy*

Abstract
The results of the application of the 3D probability tomography imaging approach to the study of the Campi Flegrei (CF) caldera are presented and discussed. The tomography approach has been applied to gravity, magnetic and ground deformation data already available in literature. The analysis of the 3D tomographic images is preceded by a brief qualitative interpretation of the original survey maps and by an outline of the probability tomography approach for each geophysical prospecting method. The results derived from the 3D tomographic images are the high occurrence probabilities of both gravity and ground deformation source centres in the CF caldera under the town of Pozzuoli. A Bouguer negative anomaly source centre is highlighted in the depth range 1.6-2 km b.s.l., whereas a positive ground deformation point source, responsible for the bradyseismic crisis of 1982-1984, is estimated at a mean depth of 3-4 km b.s.l. These inferences, combined with the results of a previous analysis of magnetotelluric, dipolar geoelectrical and self-potential data, corroborate the hypothesis that the bradyseismic events in the CF area may be explained by hot fluids vertical advection and subsequent lateral diffusion within a trapped reservoir overlying a magma chamber.

Key words *applied geophysics – potential fields – probability tomography – Campi Flegrei caldera*

1. Introduction

The Campi Flegrei (CF) volcanic area is located in South Italy around the western border of Naples. The CF volcanic history is characterized by many explosive eruptions from different vents up to the last event in 1538 A.D. with the eruption of Monte Nuovo (Rosi and Sbrana, 1987). Tectonically, the CF area is cut by a complex system of faults and fractures due to regional and local stress fields with NW-SE and NE-SW strike. Figure 1 shows a structural and volcanological sketch map of the CF area.

Geological investigations (Orsi *et al.*, 1996, 1999a) suggest that the CF area is a nested structure resulting from two major caldera-forming events. The first event was the Campanian Ignimbrite eruption 37000 years B.P. followed by the formation of a caldera with a diameter of 12-14 km. The second event was the Yellow Tuff eruption which occurred 13000 years B.P., also accompanied by a caldera collapse which began during the same eruption. The northeastern sector of this younger caldera was then affected by both widespread volcanism and block resurgence due to a simple shearing mechanism (Di Vito *et al.*, 1999). The most uplifted struc-

Mailing address: Prof. Domenico Patella, Dipartimento di Scienze Fisiche, Università «Federico II», Complesso Universitario Monte S. Angelo, Via Cinthia, 80126 Napoli, Italy; patella@na.infn.it

ture is the La Starza marine terrace along the Pozzuoli coastline. No evidence of eruptions appears offshore in the Bay of Pozzuoli, that is in the central and southern parts of the younger CF caldera.

Kinematics in the CF area is very complex, as shown by the two unrest episodes of 1969-1972 and 1982-1984. The result of these two episodes was a maximum vertical uplift of 3.5 m in the area of Pozzuoli (Berrino *et al.*, 1984).

The CF area has been little investigated with geophysical methods (Hunsche *et al.*, 1981; Monaco *et al.*, 1986; Cassano and La Torre, 1987; Barberi *et al.*, 1991; Orsi *et al.*, 1999b). Di Maio *et al.* (2000) recently performed a detailed analysis of dipole geoelectrical (DG), magnetotelluric (MT) and self-potential (SP) data sets collected over the emerged portion of the CF caldera floor. The main results are summarised as follows.

A structural outline of the CF depression was deduced from a 2D combined interpretation of MT and DG soundings along a nearly E-W profile from east of Agnano to about Cuma (see fig. 1). A 4000 $\Omega \cdot$m resistive body in the shallower 2-3 km, about 4 km wide in the E-W direction from Solfatara to southwest of Gauro, was associated with the dry volcanics of the La Starza block. It overlies a 10 $\Omega \cdot$m conductive layer of 1.5-2 km of maximum thickness, which was attributed to a trapped hot fluids reservoir, separated from the resistive overburden by an impermeable layer of similar high conductivity. Resistivity dispersion, detected only at the margins of the resistive body, was in fact ascribed to

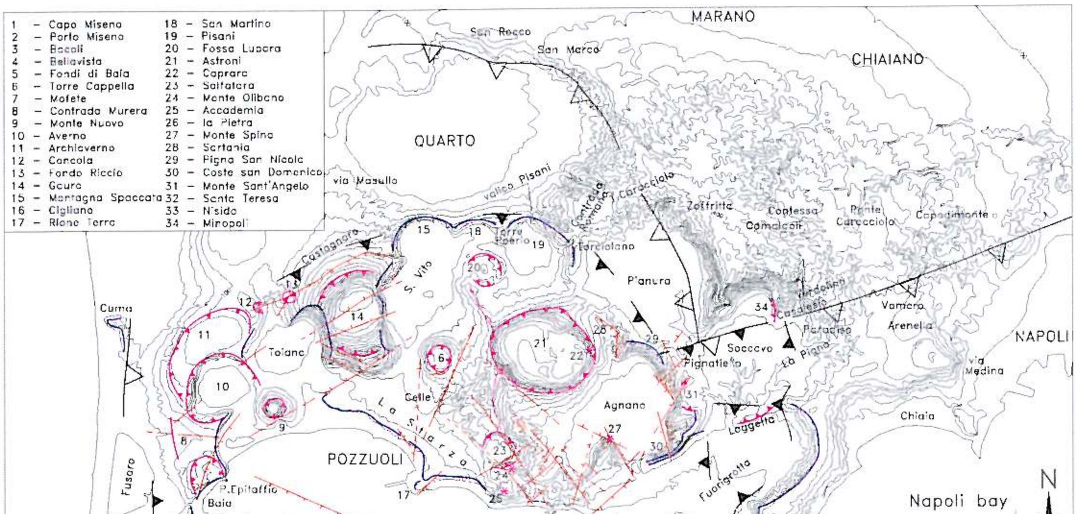

Fig. 1. A structural and volcanological sketch map of the Campi Flegrei area (after Di Vito *et al.*, 1999).

hydrothermally altered zones sealing the fracture systems bordering the resurgent La Starza block. Finally, an active pressure-temperature source at a depth not less than 5 km under the Bay of Pozzuoli was inferred from the analysis of SP data using the 3D probability tomography imaging method proposed by Patella (1997a,b).

Altogether, these results corroborate the hypothesis that the CF area must still be considered a highly hazardous volcanic system. Therefore, in order to assess a modern risk management strategy, the knowledge of its structure and dynamics needs to be further implemented, mainly within the shallowest 10 km. In this paper, we extend the geophysical investigation of the CF area by applying for the first time to gravity (GR), magnetic (MG) and ground deformation (GD) data sets the 3D probability tomography approach, formerly used for the SP analysis (Di Maio *et al.*, 2000).

2. Gravity tomography

2.1. *The CF Bouguer anomaly map*

A Bouguer anomaly (B_a) local map of the CF area was compiled by Cassano and La Torre (1987), who used a density of 1.4 g/cm^3 for slab and terrain corrections and a N35°E gradient of 0.5 mgal/km for residuation. The top slice in fig. 2 shows a scaled version of the CF residual map, obtained by further subtracting the mean B_a value in order to better distinguish negative and positive anomalies.

The main features in the map of fig. 2 are: i) an intense positive anomaly just outside the CF calderas, at the SW corner corresponding to Monte di Procida; ii) a ring of low amplitude positive anomalies along the younger CF caldera rim; iii) an intense negative anomaly inside the CF calderas, mostly offshore in the Bay of Pozzuoli.

2.2. *Gravity source centres tomography*

The scaled residual B_a map was analysed by a new probability tomography method aimed at imaging the 3D configuration of GR sources (Mauriello and Patella, 2001a,b). An outline of the method follows.

Consider a coordinate system with the (x,y)-plane at sea level and the z-axis positive downwards. The $B_a(\mathbf{r})$ value measured at an observation point $\mathbf{r}$ on a surface S characterized by a height function $z(x,y)$ a.s.l. is assumed to be due to the superposition of Q partial effects, say

$$B_a(\mathbf{r}) = \sum_{q=1}^{Q} \Gamma_q \, s(\mathbf{r}_q - \mathbf{r}) \tag{2.1}$$

where

$$s(\mathbf{r}_q - \mathbf{r}) = \frac{z_q - z}{\left|\mathbf{r}_q - \mathbf{r}\right|^3} \tag{2.2}$$

The q-th element has strength Γ_q equal to the gravitational constant G times the excess or deficit of mass concentrated at a point $\mathbf{r}_q \equiv (x_q, y_q, z_q)$.

Using eq. (2.1), the power Λ associated with $B_a(\mathbf{r})$ over S is written as

$$\Lambda = \int_S B_a^2(\mathbf{r})dS = \sum_{q=1}^{Q} \Gamma_q \int_S B_a(\mathbf{r})s(\mathbf{r}_q - \mathbf{r})dS. \tag{2.3}$$

Application of Schwarz's inequality to the q-th integral in eq. (2.3) leads to

$$\left[\int_{-X}^{X}\int_{-Y}^{Y} B_a(\mathbf{r})s(\mathbf{r}_q - \mathbf{r})g(z)dxdy\right]^2 \leq \tag{2.4}$$

$$\leq \int_{-X}^{X}\int_{-Y}^{Y} B_a^2(\mathbf{r})g(z)dxdy \int_{-X}^{X}\int_{-Y}^{Y} s^2(\mathbf{r}_q - \mathbf{r})g(z)dxdy$$

where it was assumed that the projection of S onto the (x, y)-plane can always be adapted to a rectangle with sides $2X$ and $2Y$ along the x- and y-axis, respectively. The projection from the actual surface S to the rectangle $[2X, 2Y]$ requires a topographic surface regularization factor $g(z)$

expressed by

$$g(z)=\sqrt{1+(\partial z/\partial x)^2+(\partial z/\partial y)^2}\,. \qquad (2.5)$$

From eq. (2.4) a function $\eta(\boldsymbol{r}_q)$ can be defined as (Mauriello and Patella, 2001a,b)

$$\eta(\boldsymbol{r}_q)=C_q\int_{-X}^{X}\int_{-Y}^{Y}B_a(\boldsymbol{r})s(\boldsymbol{r}_q-\boldsymbol{r})g(z)dxdy \qquad (2.6)$$

$$\text{with}\quad -1\le\eta(\boldsymbol{r}_q)\le+1$$

where

$$C_q = \qquad (2.7)$$

$$=\left\{\int_{-X}^{X}\int_{-Y}^{Y}B_a^2(\boldsymbol{r})g(z)dxdy\int_{-X}^{X}\int_{-Y}^{Y}s^2(\boldsymbol{r}_q-\boldsymbol{r})g(z)dxdy\right\}^{-1/2}.$$

The function $\eta(\boldsymbol{r}_q)$ is interpreted as the probability a positive ($\eta>0$) or negative ($\eta<0$) Δ-mass source located at $\boldsymbol{r}_q$ obtains as responsible of the observed GR field. A 3D tomographic image of this probability function can be thus constructed by scanning the subsurface *e.g.*, along a sequence of horizontal slices at different depths. This 3D image can then be used to retrieve a likely distribution of buried Δ-mass sources fitting the observed $B_a(\boldsymbol{r})$ map in a probabilistic sense.

The results of this approach in the CF area are depicted in fig. 2. Left- and right-hand sequences of slices below the reference B_a map show the GR sources images at depths b.s.l. from 0.4 km to 2 km and from 2 km to 6 km, respectively.

In addition to the circular sequence of positive Δ-mass sources appearing along the younger CF caldera rim in the first 0.8 km b.s.l. and distributed almost continuously in the western side of the area, the 3D probability tomography discloses the following two main features. The first is a positive Δ-mass nucleus with η-values close to + 0.8, appearing at the southwestern corner of the slices in the depth range 0.4-4 km b.s.l., in correspondence of Monte di Procida (see fig. 1 for geographic reference). The second feature is a negative nucleus with η-values close to – 1, appearing in the central area in the depth range 1.6-2 km b.s.l., beneath the town of Pozzuoli.

2.3. *Gravity source boundaries tomography*

To further investigate the CF GR residual map, we used a Δ-mass dipole tomography imaging approach aimed at highlighting the 3D probability distribution of the density contrast interfaces (Iuliano *et al.*, 2001). We assume, in fact, that any density discontinuity can be locally assimilated to a Δ-mass double layer, *i.e.* to a distribution of Δ-mass dipoles located across the interface. Generalising, we can assume that among the sources of the GR field there are P dipoles with moment $\boldsymbol{d}_p$ ($p=1,2,...,P$), whose total vertical GR field is written as

$$B_a^{(d)}(\boldsymbol{r})=\sum_{p=1}^{P}(\boldsymbol{d}_p\cdot\nabla_p)s(\boldsymbol{r}_p-\boldsymbol{r}). \qquad (2.8)$$

We extract from the total power Λ, given in eq. (2.3), the contribution $\Lambda^{(d)}$ due to $B_a^{(d)}(\boldsymbol{r})$ and write it as (Iuliano *et al.*, 2001)

$$\Lambda^{(d)}=\sum_{p=1}^{P}\sum_{v=x,y,z}d_{pv_p}\int_S B_a(\boldsymbol{r})\frac{\partial s(\boldsymbol{r}_p-\boldsymbol{r})}{\partial v_p}dS. \qquad (2.9)$$

Application of Schwarz's inequality to the p-th term of eq. (2.9) allows a 3D Δ-mass dipole probability of occurrence function to be now defined as

$$\eta_v(\boldsymbol{r}_p)= \qquad (2.10)$$

$$=C_{pv}\int_{-X}^{X}\int_{-Y}^{Y}B_a(\boldsymbol{r})\frac{\partial s(\boldsymbol{r}_p-\boldsymbol{r})}{\partial v_p}g(z)dxdy,\quad v=x,y,z,$$

with

$$C_{pv} =$$

$$=\left\{\int_{-X}^{X}\int_{-Y}^{-Y}B_a^2(\boldsymbol{r})g(z)dxdy\int_{-X}^{X}\int_{-Y}^{Y}\left|\frac{\partial s(\boldsymbol{r}_p-\boldsymbol{r})}{\partial v_p}\right|^2 g(z)dxdy\right\}^{-1/2}, \qquad (2.11)$$

$$v=x,y,z.$$

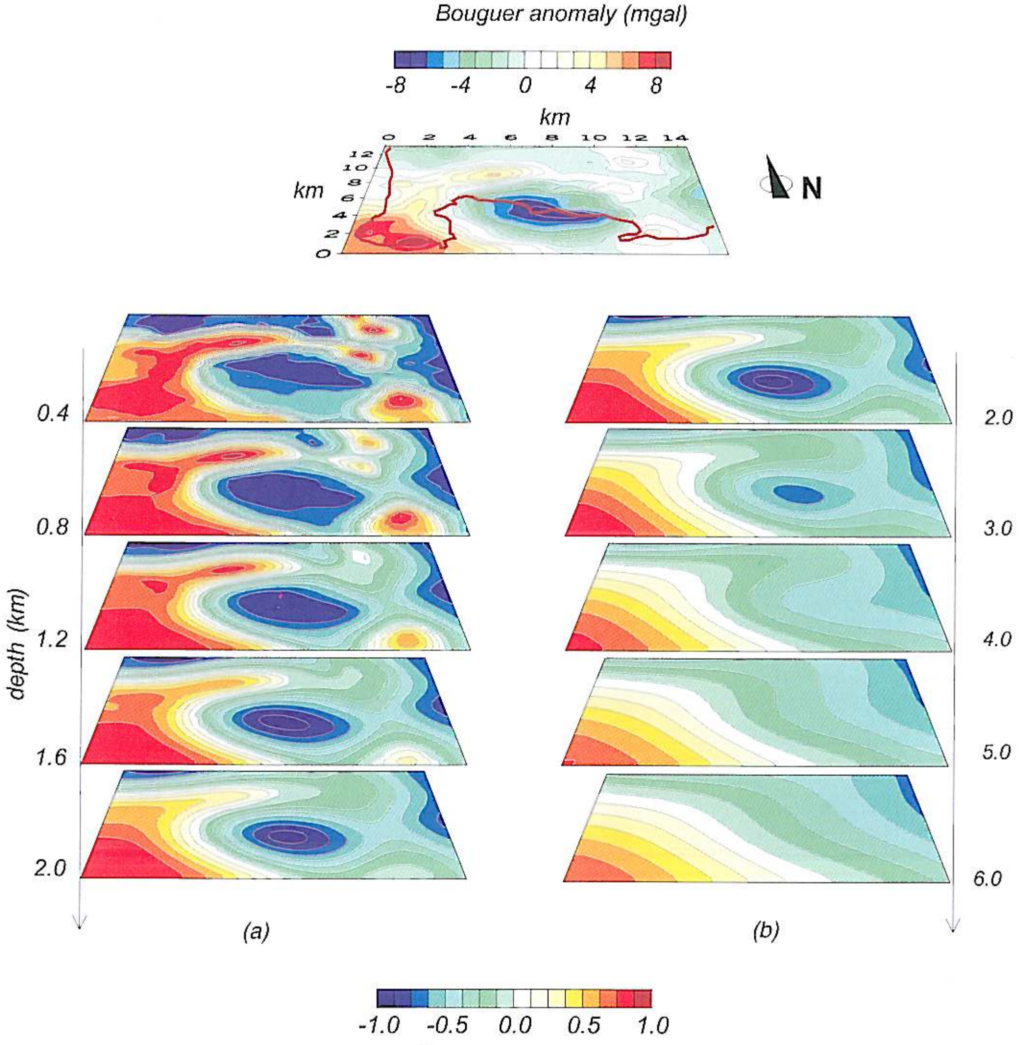

Fig. 2. The gravity source centres probability tomography in the depth ranges 0.4-2 km b.s.l. (*a*) and 2-6 km b.s.l. (*b*). The top slice is the residual Bouguer anomaly survey map (after Cassano and La Torre, 1987).

Thus, at each $\boldsymbol{r}_p$, three occurrence probability values, say η_x, η_y and η_z, can be calculated. Each value gives the probability with which the relative component of the Δ-mass dipole located at $\boldsymbol{r}_p$ is responsible for the observed GR field.

Figures 3a-c show the results of this new tomographic approach to the analysis of the CF GR data set. In particular, figs. 3a, 3b and 3c show the η_x, η_y and η_z distribution patterns, respectively. The left- and right-hand sequences of slices below the reference B_a map show the 3D GR

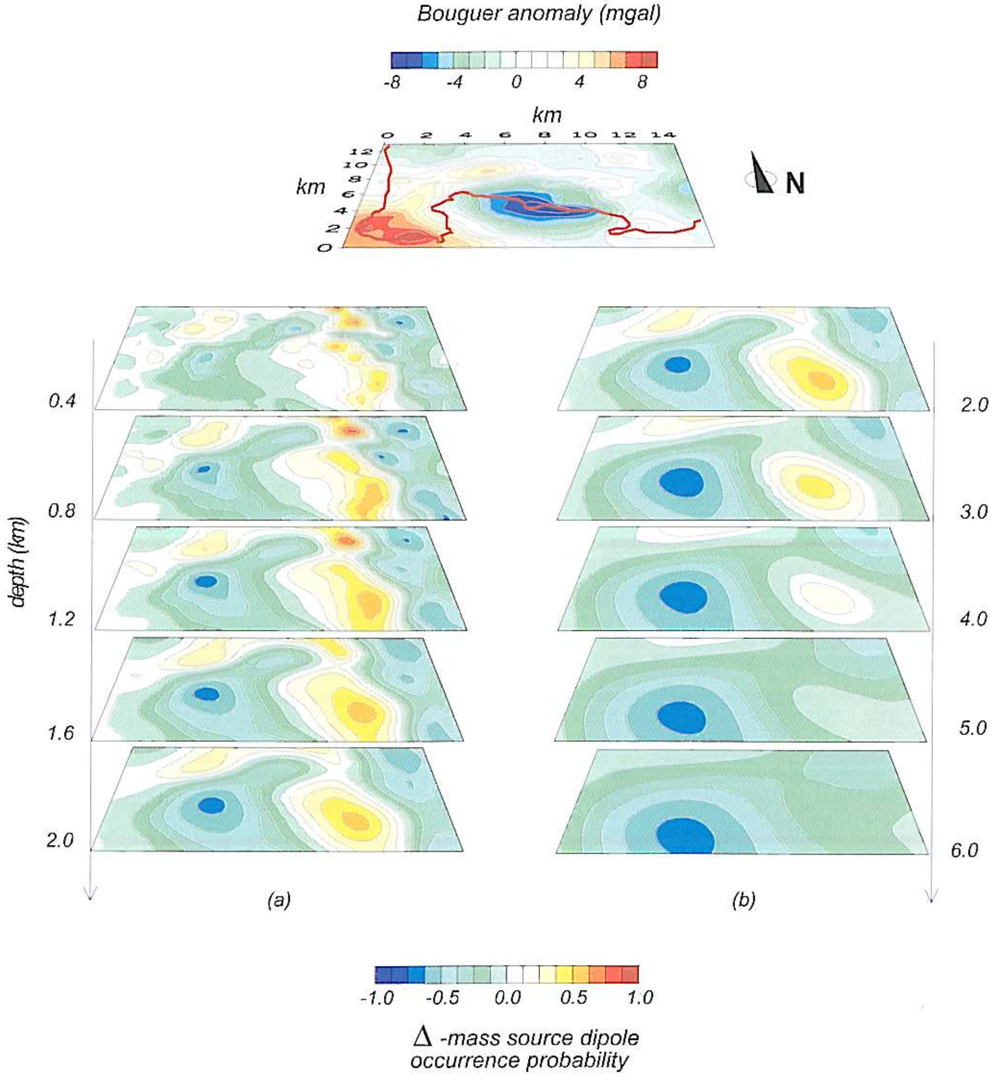

Fig. 3a. The gravity source boundaries probability tomography in the depth ranges 0.4-2 km b.s.l. (*a*) and 2-6 km b.s.l. (*b*) for the *x*-component of the source dipole occurrence probability function. The top slice is the residual Bouguer anomaly survey map (after Cassano and La Torre, 1987).

source boundary images at depths b.s.l. from 0.4 km to 2 km and from 2 km to 6 km, respectively. The η_x and η_y Δ-mass dipole tomographies (figs. 3a and 3b, respectively) give a clear picture of the lateral boundaries of the CF depression along the W-E (x-axis) and S-N (y-axis) directions, respectively. Generally, the highest probabilities occur at a depth of about 2 km, except for the boundary between the Monte di Procida dense structure and the light volcanics inside the CF caldera, which extends down to much greater depths. The η_z Δ-mass dipole

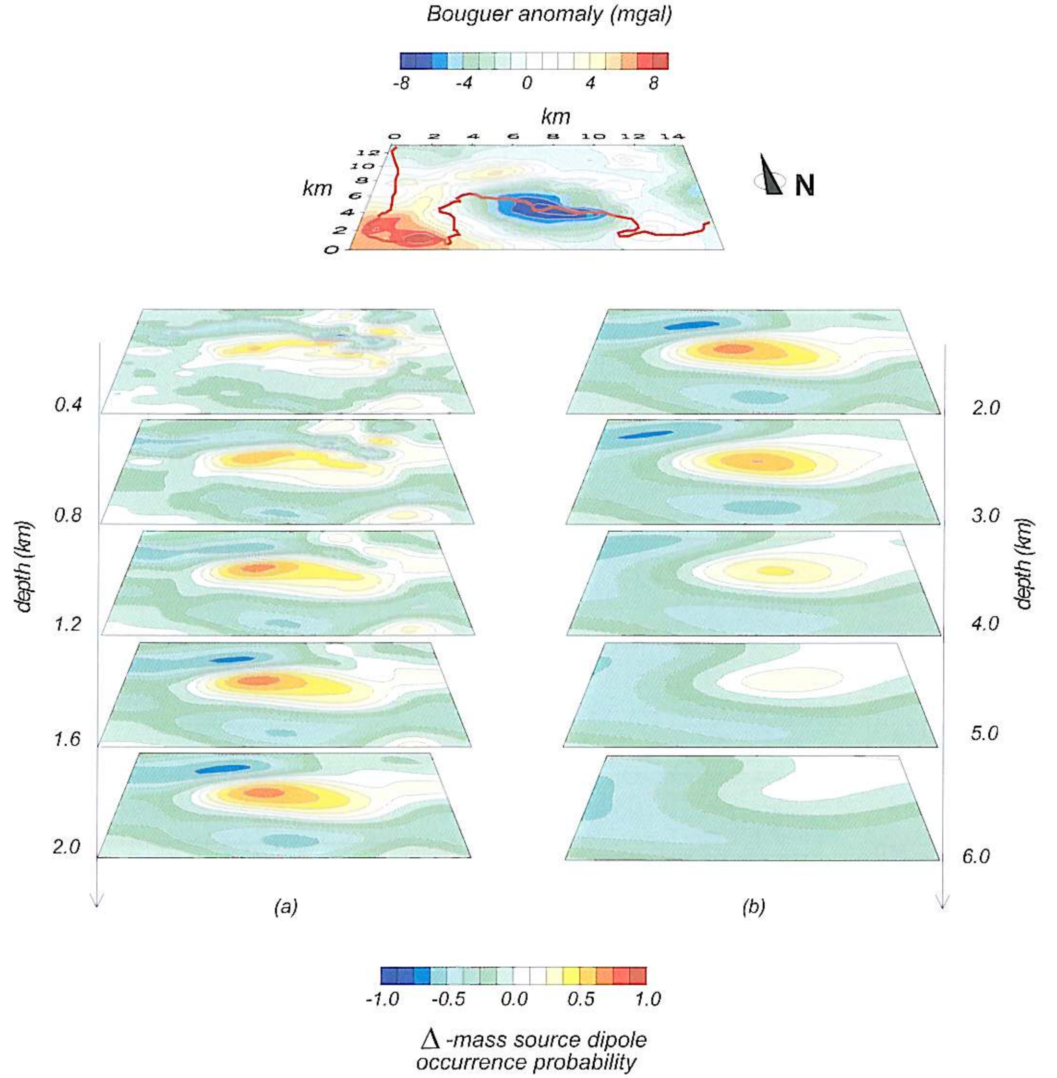

Fig. 3b. The gravity source boundaries probability tomography in the depth ranges 0.4-2 km b.s.l. (*a*) and 2-6 km b.s.l. (*b*) for the *y*-component of the source dipole occurrence probability function. The top slice is the residual Bouguer anomaly survey map (after Cassano and La Torre, 1987).

tomography (fig. 3c) shows, instead, a pattern very similar to that of the Δ-mass source tomography of fig. 2. In fact, the GR effect of a Δ-mass vertical dipole cannot be distinguished from the effect of a Δ-mass single pole replacing the vertical dipole.

3. Magnetic tomography

3.1. *The CF magnetic anomaly map*

For the MG analysis of the CF area we used a data set derived from the aeromagnetic survey

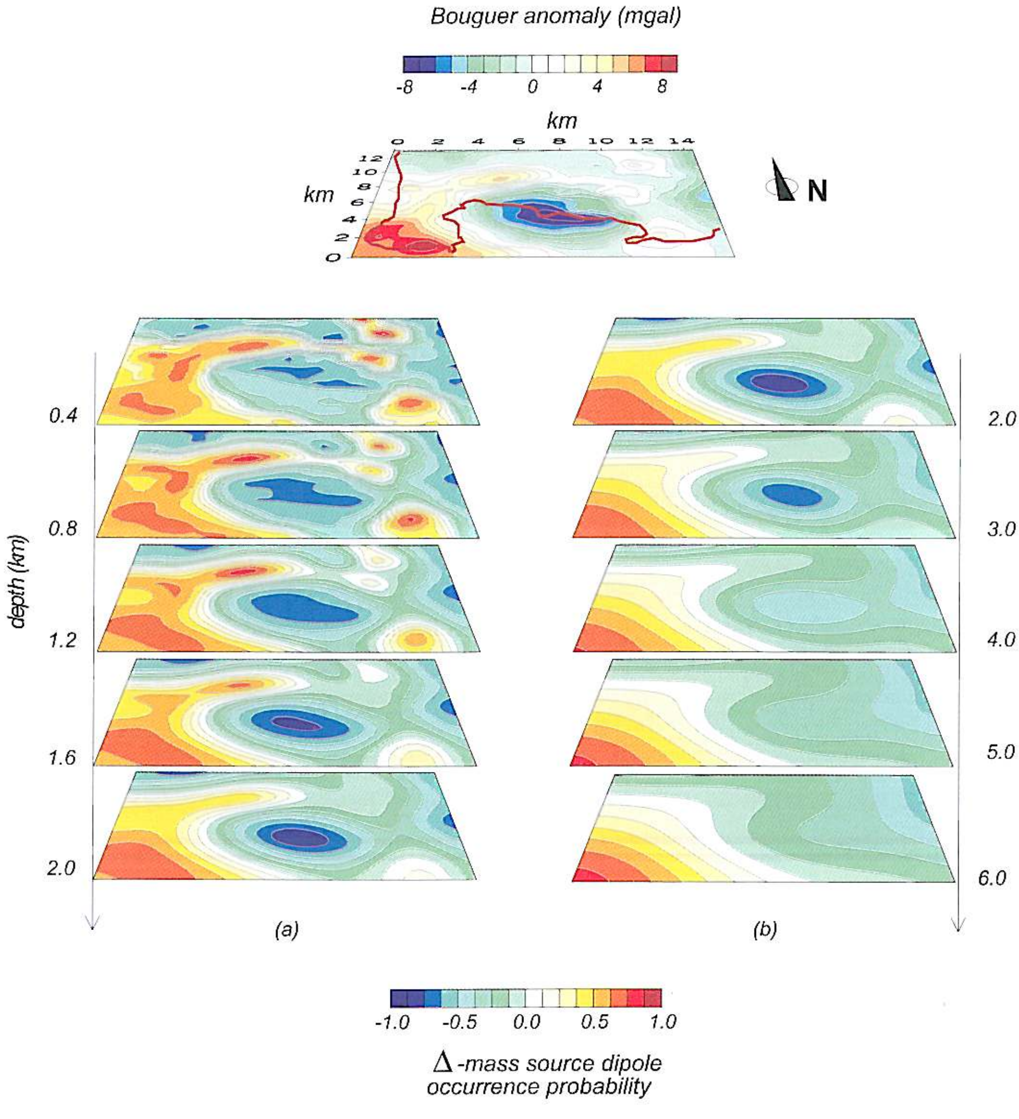

Fig. 3c. The gravity source boundaries probability tomography in the depth ranges 0.4-2 km b.s.l. (*a*) and 2-6 km b.s.l. (*b*) for the *z*-component of the source dipole occurrence probability function. The top slice is the residual Bouguer anomaly survey map (after Cassano and La Torre, 1987).

carried out in 1977 by the Italian Oil Company AGIP (Cassano and La Torre, 1987). A caesium optical pumping magnetometer was used to measure the total field intensity at a constant flight altitude of 1460 m.

The top slice in fig. 4 shows the residual MG total field map. The main features are two strong highs, one in the area of Monte di Procida and the other in the Astroni-Agnano area.

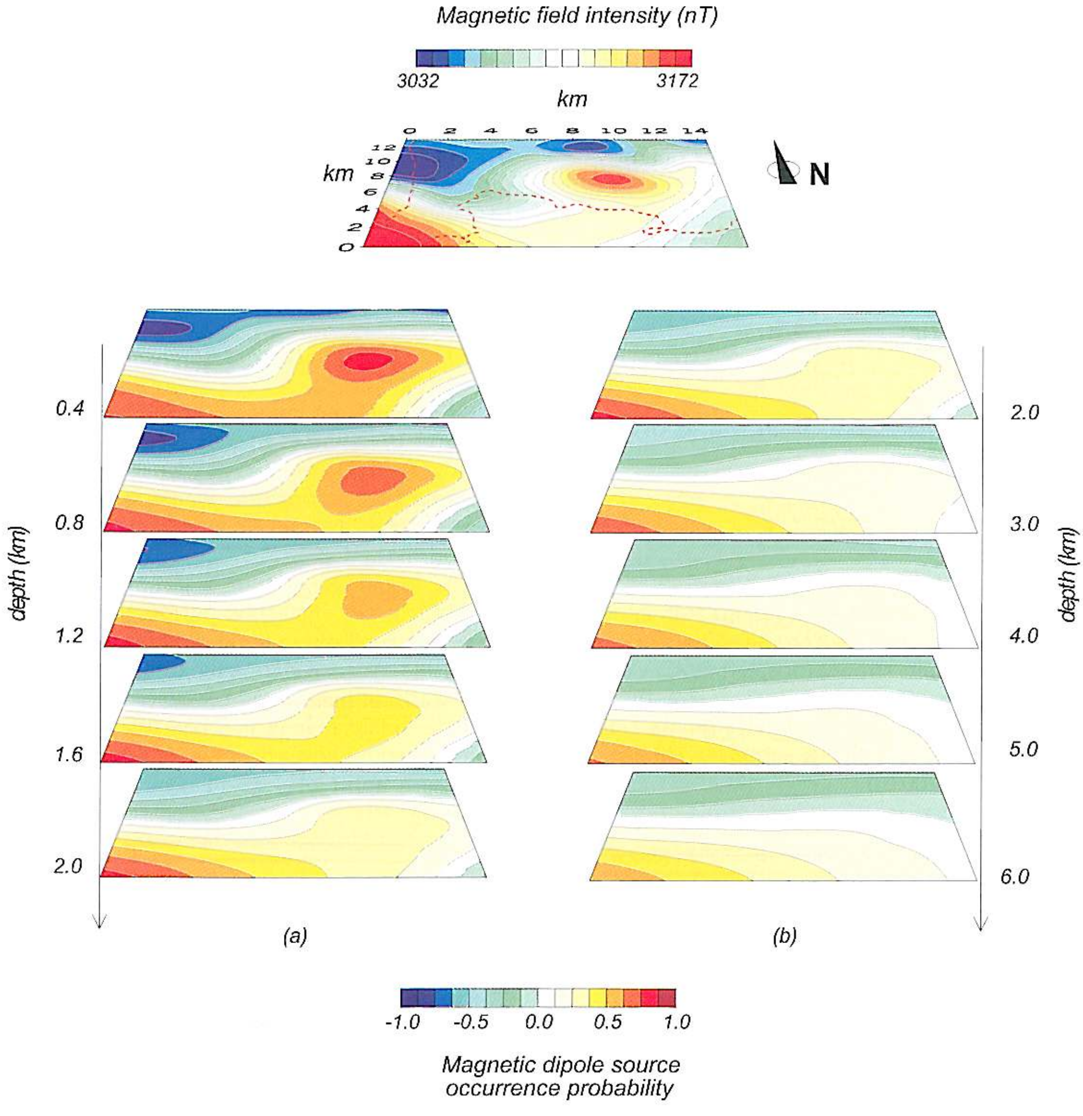

Fig. 4. The magnetic dipole source centres probability tomography in the depth ranges 0.4-2 km b.s.l. (*a*) and 2-6 km b.s.l. (*b*). The top slice is the residual total aeromagnetic field map (after Cassano and La Torre, 1987).

3.2. *Magnetic dipole source tomography*

Because the MG data are usually collected as total field intensities, as in the case of the CF study, a modification of the tomographic procedure was necessary. In fact, a linear superposition of source effects as in eq. (2.1) is now not possible. We followed the procedure of Mauriello and Patella (2001c), which is briefly outlined.

We denote with H the difference between the modulus of the measured MG field and the modulus of a reference primary field and expand H in a Taylor series of the magnetic moment increments $\Delta \boldsymbol{m}_q$. Truncating the series to the first partial derivative terms, we obtain

$$H(\boldsymbol{r}) = \sum_{q=1}^{Q} \left[\frac{\partial H(\boldsymbol{r})}{\partial m_{qx}} \Delta m_{qx} + \frac{\partial H(\boldsymbol{r})}{\partial m_{qy}} \Delta m_{qy} + \frac{\partial H(\boldsymbol{r})}{\partial m_{qz}} \Delta m_{qz} \right]. \tag{3.1}$$

The total power Λ associated with H over S is written as

$$\Lambda = \sum_{q=1}^{Q} \sum_{v=x,y,z} \Delta m_{qv} \int_S H(\boldsymbol{r}) s_v(\boldsymbol{r}_q - \boldsymbol{r}) dS \tag{3.2}$$

where the function $s_v(\boldsymbol{r}_q - \boldsymbol{r})$ is the v-th component of the MG field at $\boldsymbol{r}$ produced by a magnetic dipole of unit strength located at $\boldsymbol{r}_q$.

Using the same procedure as for the GR tomography, we define the MG dipole source occurrence probability function as (Mauriello and Patella, 2001c)

$$\eta_v(\boldsymbol{r}_q) = C_{qv} \int_{-X}^{X} \int_{-Y}^{Y} H(\boldsymbol{r}) s_v(\boldsymbol{r}_q - \boldsymbol{r}) g(z) dx dy \tag{3.3}$$

where $g(z)$ is the same surface regularization factor used in the GR tomography.

Thus, at each $\boldsymbol{r}_q$ three η values can be obtained, say η_x, η_y and η_z. These values give the probabilities with which the three components of a MG dipole source at $\boldsymbol{r}_q$ are responsible for the observed anomalous field.

The application of this imaging approach to the CF MG map is shown in fig. 4. In order to avoid useless dispersion of data, a unique 3D picture was elaborated by assigning at each $\boldsymbol{r}_q$ the highest absolute value among the three probabilities η_x, η_y, η_z, taken with its actual sign. The left-hand and right-hand sequences of slices below the reference aeromagnetic survey map show the 3D MG source dipole tomographies at depths b.s.l. from 0.4 km to 2 km and from 2 km to 6 km, respectively. The conclusions drawn from these plots are the high probabilities of occurrence of MG dipole sources south of Monte di Procida in the depth interval 0.8-2 km b.s.l. and in the Astroni-Agnano area at a depth not exceeding 0.4 km b.s.l. In both areas, the secondary MG dipole source would be aligned in such a way as to enhance the local MG primary field.

4. Ground deformation tomography

4.1. *The CF ground deformation anomaly maps*

GD monitoring in the CF area started during the 1969-1972 unrest episode. Vertical GD data are now routinely provided by a network of 124 benchmarks covering the whole area subject to resurgence and subsidence cycles (Berrino *et al.*, 1984).

The top slices of figs. 5 through 10 show the vertical GD measured during six different surveys carried out in the period January 1983-June 1984. At each station the reference ground level was that measured in January 1982. In all maps the main feature is a nearly circular GD anomaly centred over the town of Pozzuoli with maximum uplift of 1.79 m occurred on June 1984 (fig. 10).

4.2. *Ground deformation source tomography*

GD in volcanic areas is usually interpreted as the response of an elastic medium to a pressure increase in a magma chamber or to a magma intrusion (Mogi, 1958). However, large GD values in small areas without any apparent intrusion, as was the case in the CF area during the 1982-1984 unrest episode, would imply an unreasonably large pressure increase (Bianchi *et al.*, 1986). Bonafede (1991) suggested a thermal advection mechanism to explain abnormal GD values in volcanic areas. He considered a pressure-temperature increase within a confined fluids reservoir producing a system of connected fractures during fluid migration towards the top boundary of the reservoir. Numerical simulations demonstrated that forced advection of hot fluids can be a very efficient GD source.

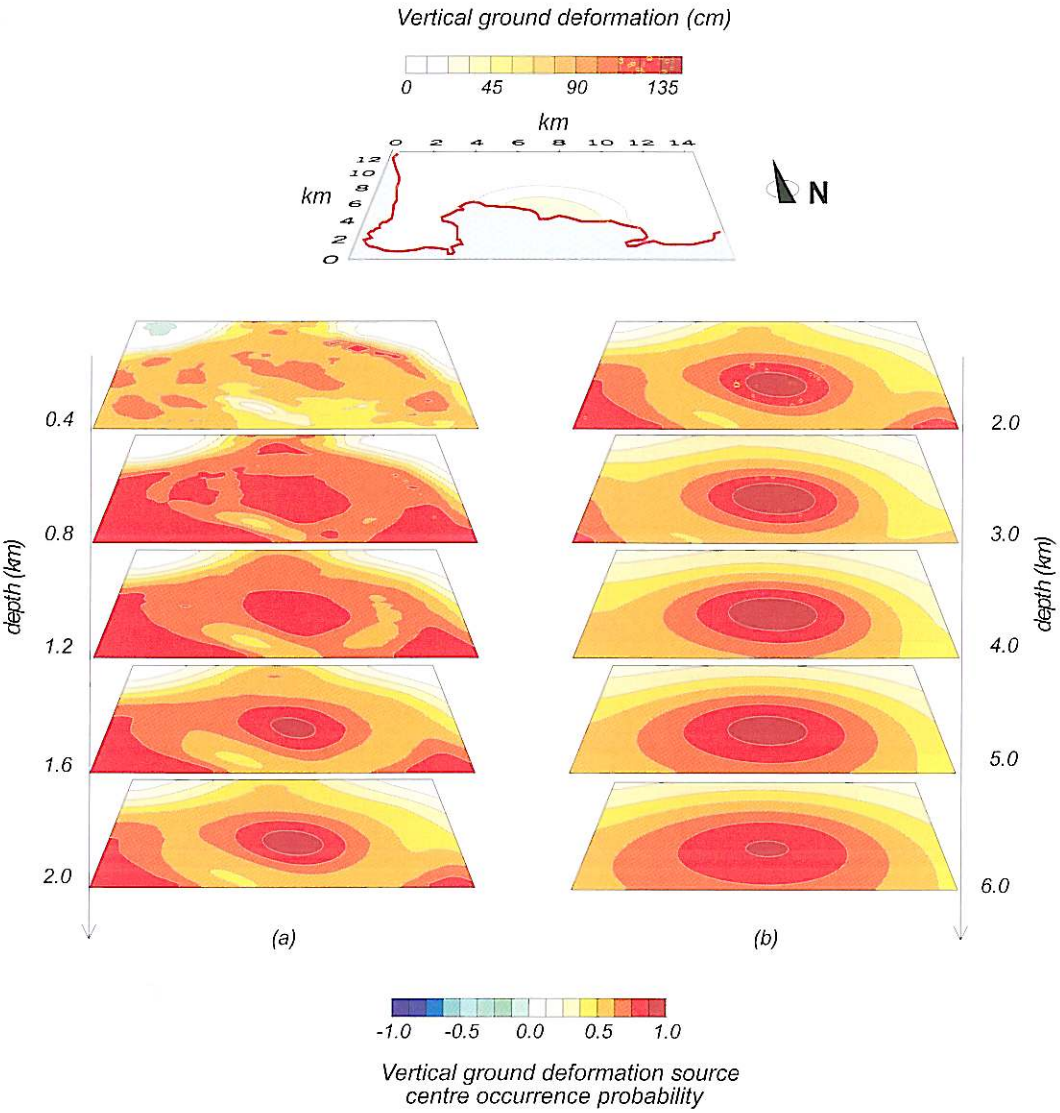

Fig. 5. The vertical ground deformation source centres probability tomography in the depth ranges 0.4-2 km b.s.l. (*a*) and 2-6 km b.s.l. (*b*). The top slice is the vertical ground deformation field map referred to the survey of January 1983 (after Berrino *et al.*, 1984).

In order to image the distribution of GD sources in the CF area, we have adapted our probability tomography approach starting from the hot fluids model of Bonafede (1991) as follows. We put with mod_0 a reference model supposed to be a homogeneous, elastic and porous medium. If a small volume around a point $\boldsymbol{r}_q$ of the subsoil is affected by a pressure and/or temperature variation, a point $\boldsymbol{r}$ at the ground surface is displaced by an amount $\delta h(\boldsymbol{r})$ equal

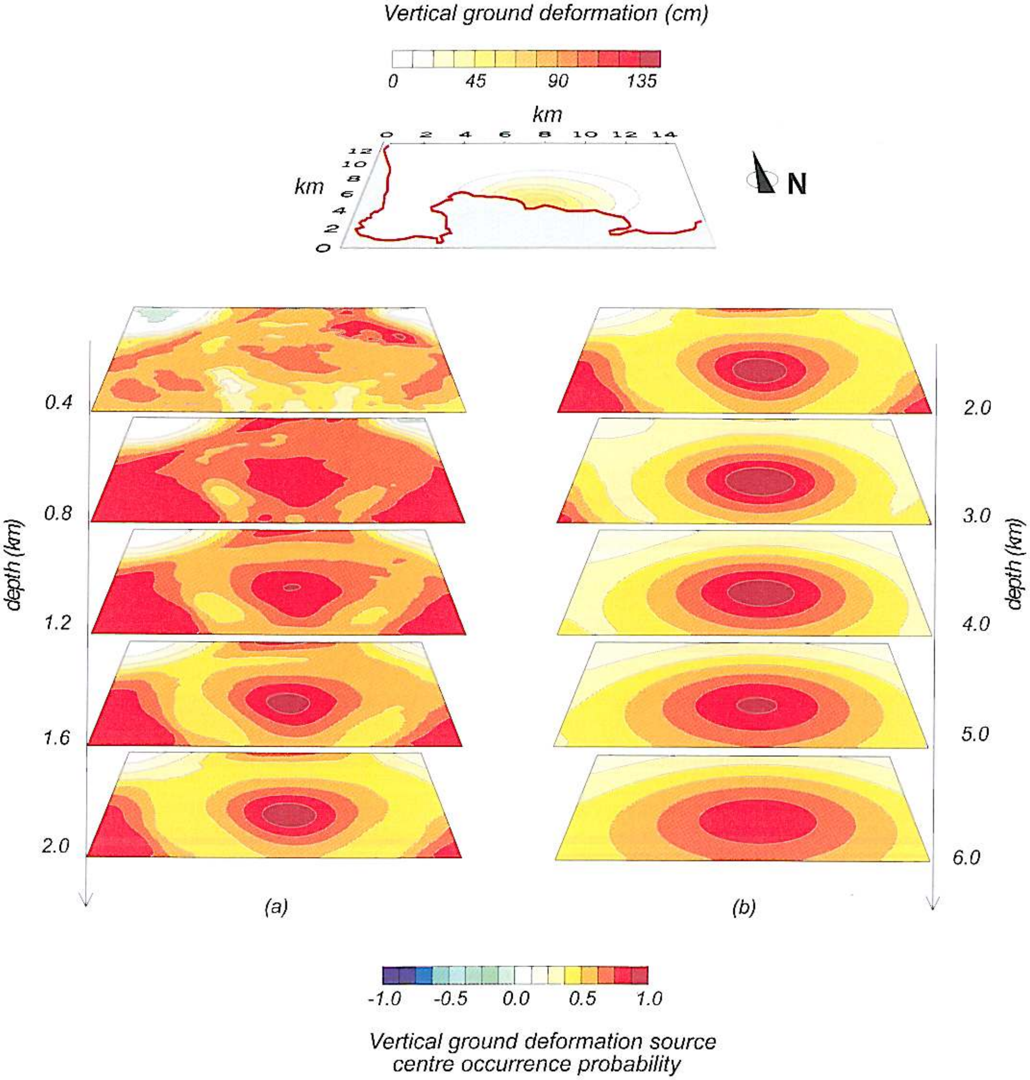

Fig. 6. The vertical ground deformation source centres probability tomography in the depth ranges 0.4-2 km b.s.l. (*a*) and 2-6 km b.s.l. (*b*). The top slice is the vertical ground deformation field map referred to the survey of June 1983 (after Berrino *et al.*, 1984).

to (Bonafede, 1991)

$$\delta h(\boldsymbol{r}) = \frac{\delta M_q (z_q - z)}{4\mu |\boldsymbol{r}_q - \boldsymbol{r}|^3} \tag{4.1}$$

where μ is the rigidity modulus of mod_0 and δM_q is a coefficient depending on pressure and temperature in the source element and on the properties of mod_0 (Poisson's ratio, diffusivity and pore pressure). The z-axis is positive downwards.

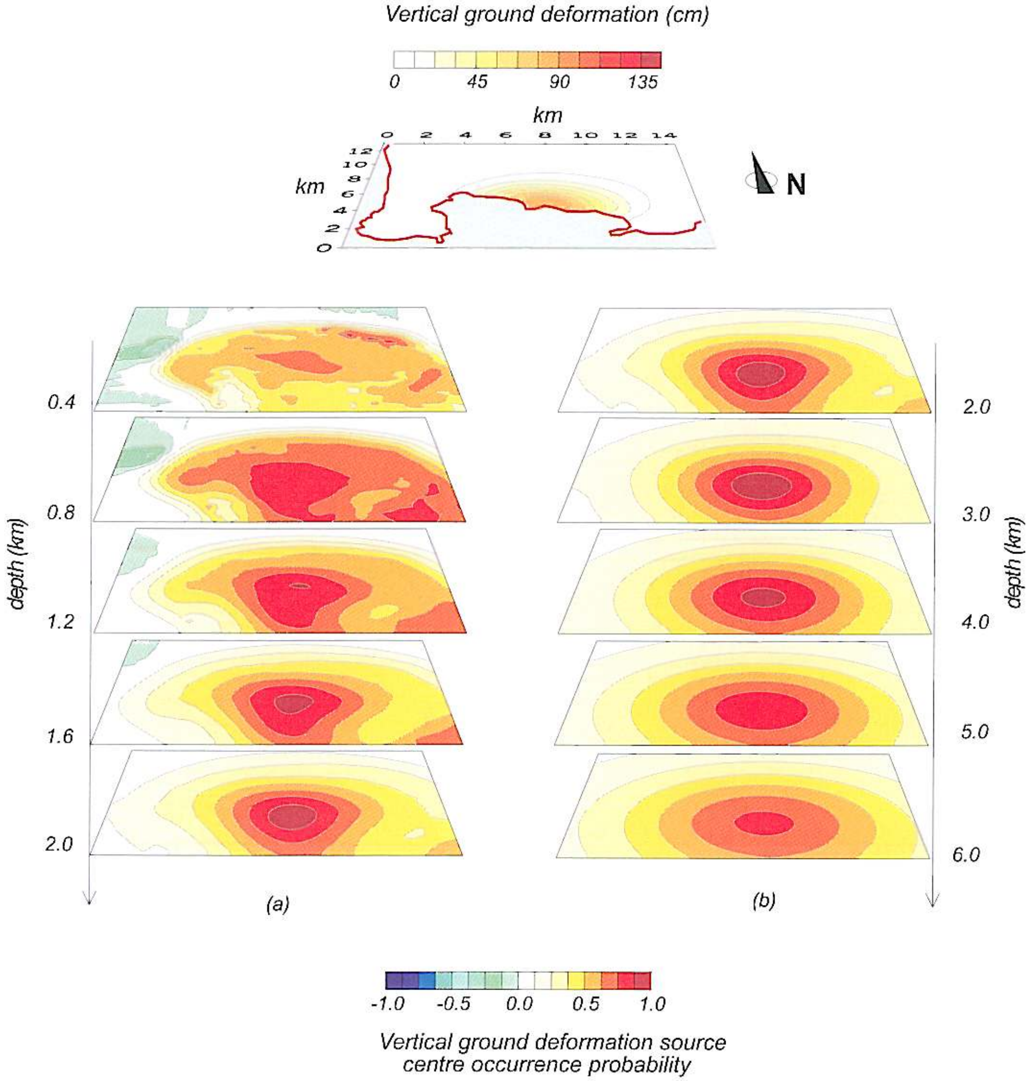

Fig. 7. The vertical ground deformation source centres probability tomography in the depth ranges 0.4-2 km b.s.l. (*a*) and 2-6 km b.s.l. (*b*). The top slice is the vertical ground deformation field map referred to the survey of September 1983 (after Berrino *et al.*, 1984).

Expanding the observed $h(\boldsymbol{r})$ function in a Taylor series we obtain

$$h(\boldsymbol{r}) = \sum_{q=1}^{Q} \frac{\delta h(\boldsymbol{r})}{\delta M_q} \delta M_q + \textit{higher order terms}. \tag{4.2}$$

Higher order terms contain information about the actual nature of the subsurface (*e.g.*, presence of shallow aquifers) and can be calculated by introducing appropriate coefficients, which are generally unknown in advance. However, since we are interested in imaging only the oc-

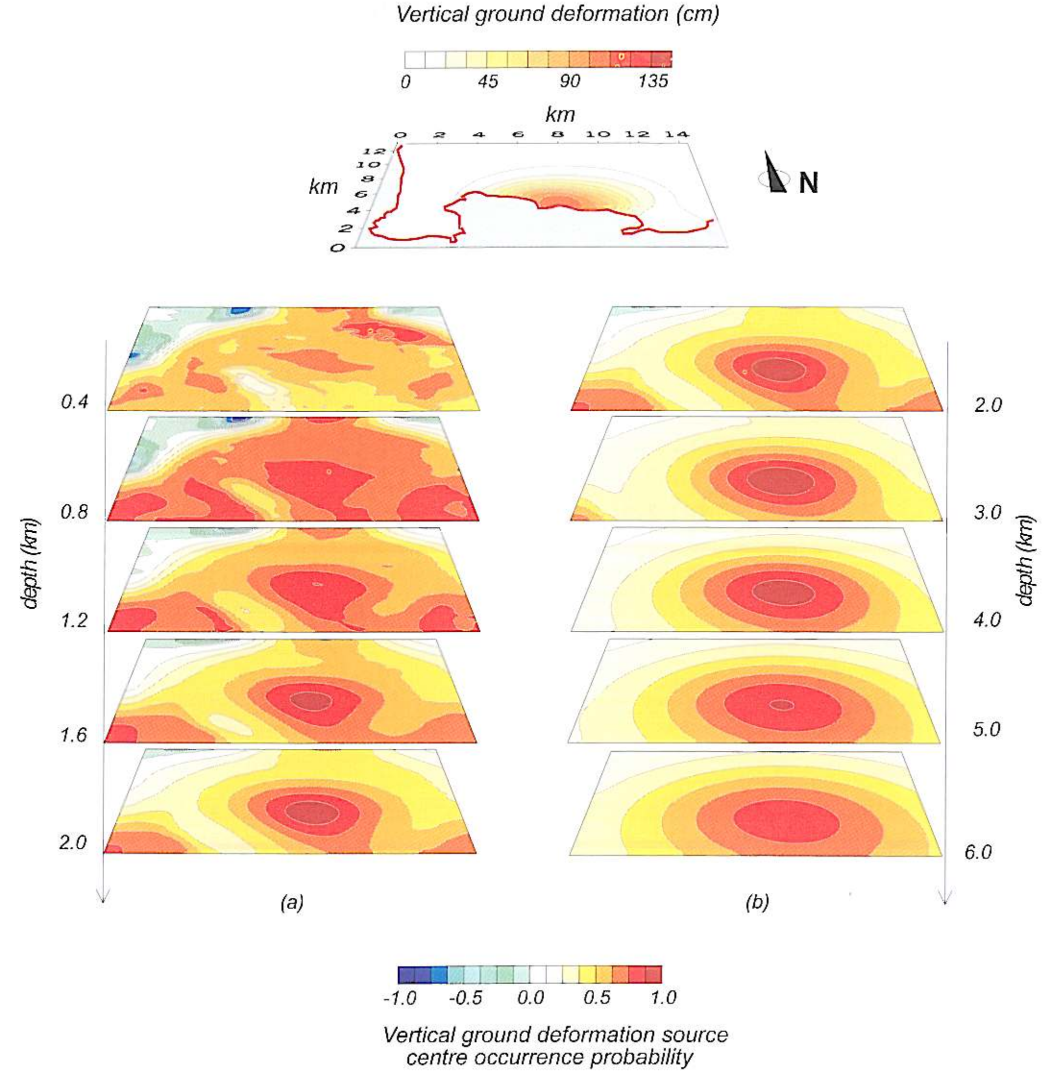

Fig. 8. The vertical ground deformation source centres probability tomography in the depth ranges 0.4-2 km b.s.l. (*a*) and 2-6 km b.s.l. (*b*). The top slice is the vertical ground deformation field map referred to the survey of December 1983 (after Berrino *et al.*, 1984).

currence probability distribution of hot fluids source elements, we can limit the analysis only to the first order terms.

Therefore, following the same procedure as in the previous sections, we define the occurrence probability function $\eta(\boldsymbol{r}_q)$ for GD source analysis as

$$\eta(\boldsymbol{r}_q) = C_q \int_{-X}^{X} \int_{-Y}^{Y} h(\boldsymbol{r}) s(\boldsymbol{r}_q - \boldsymbol{r}) g(z) dx dy \qquad (4.3)$$

where $s(\boldsymbol{r}_q - \boldsymbol{r})$ is expressed by eq. (2.2) and

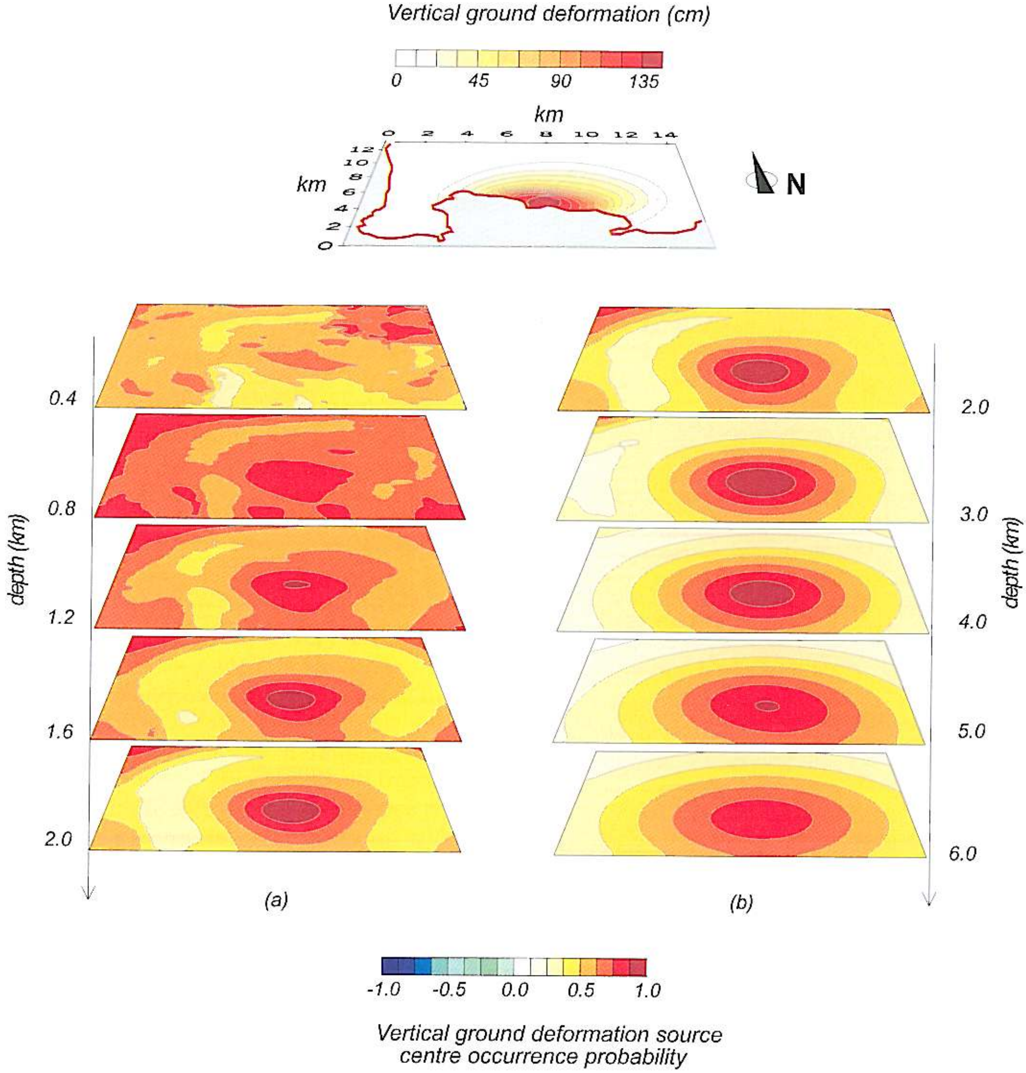

Fig. 9. The vertical ground deformation source centres probability tomography in the depth ranges 0.4-2 km b.s.l. (*a*) and 2-6 km b.s.l. (*b*). The top slice is the vertical ground deformation field map referred to the survey of March 1984 (after Berrino *et al.*, 1984).

$$C_q = \tag{4.4}$$

$$= \left\{ \int_{-X}^{X}\int_{-Y}^{Y} h^2(\mathbf{r})g(z)dxdy \int_{-X}^{X}\int_{-Y}^{Y} s^2(\mathbf{r}_q - \mathbf{r})g(z)dxdy \right\}^{-1/2}.$$

The results of the application of this GD tomographic approach to the CF data are depicted in figs. 5 through 10. The left- and right-hand sequences of slices beneath the reference GD survey maps show the source images at depths b.s.l. from 0.4 km to 2 km and from 2 km to 6 km, respec-

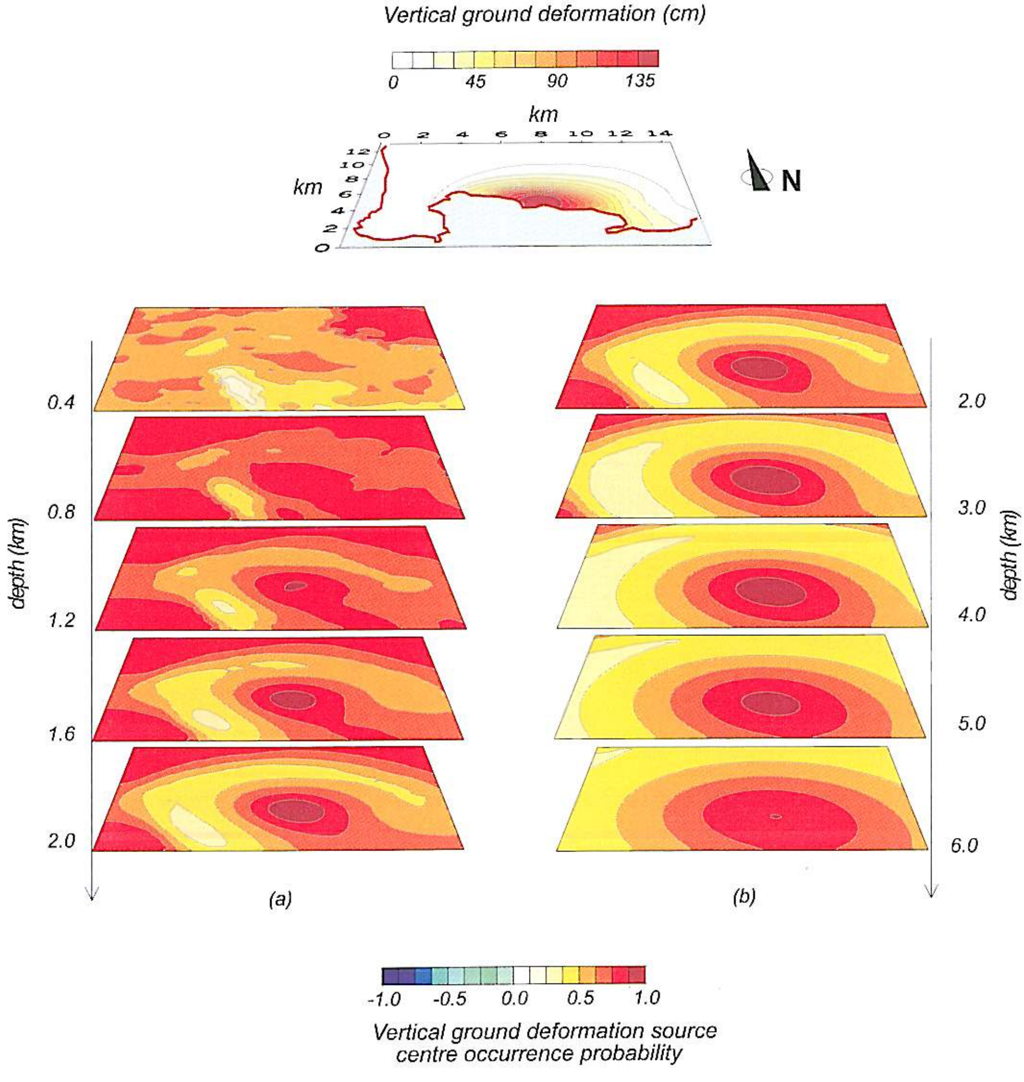

Fig. 10. The vertical ground deformation source centres probability tomography in the depth ranges 0.4-2 km b.s.l. (*a*) and 2-6 km b.s.l. (*b*). The top slice is the vertical ground deformation field map referred to the survey of June 1984 (after Berrino *et al.*, 1984).

tively. The conclusion drawn from this time sequence of 3D plots is the recurrent presence of high values of the η-function about in the same place under the town of Pozzuoli. The highest occurrence probabilities of a pressurised hot fluids equivalent point source are estimated at 3-4 km b.s.l.

5. Discussion and conclusions

Compiling the results from the previous SP tomographic imaging (Di Maio *et al.*, 2000) and the present GR and GD tomographic images, the following features are outlined in terms of point sources:

a) A pressure-temperature source centre not less than 5 km deep accounts for the wide negative nucleus shown by the SP tomography under the Bay of Pozzuoli.

b) A pressure-temperature source centre at around 3-4 km of depth explains the notably less extended positive nucleus shown by the ground deformation tomography under the Bay of Pozzuoli (figs. 5 through 10).

c) A mass deficit source centre at a depth around 2 km accounts for the negative nucleus shown by the GR tomography under the Bay of Pozzuoli (fig. 2).

Bianchi *et al.* (1986) maintain that exceedingly high ground uplifts, like those detected in the CF area (over 1.7 m in both crises of 1969-1972 and 1982-1984) without any apparent magma intrusion, cannot be explained by pressure increase in a shallow magma chamber. Bonafede (1991) suggested that forced advection of hot fluids in a reservoir overlying a magma chamber can be a very efficient GD source. Furthermore, Orsi *et al.* (1999c) maintain that hot fluids advection can account for the intense seismic activity during uplift and its absence during subsidence. Earthquakes during resurgence would be associated with fracturing, whereas their absence during subsidence would be explained by lateral fluid diffusion without regression of source pressures.

Combining these last phenomenological aspects with the results of the potential fields tomographies, we can suggest the following conclusions:

a) The SP source with hypocentral location at a depth not less than 5 km may be related to a primary source structure, *e.g.* a magma chamber. Electric currents can in fact be generated by temperature gradients (Thomson effect) and/or pressure gradients (streaming potential) without necessarily invoking a massive fluid motion (Di Maio and Patella, 1991).

b) The GD tomographies clearly show a source for ground uplift centered at a depth around 3-4 km. We can thus corroborate the hypothesis of existence of a shallower geothermal reservoir, where hot fluid advection is activated due to heating from an underlying heat source (magma chamber).

c) The GR tomography allows the observed B_a low under the Bay of Pozzuoli to be explained in terms of a less dense body with hypocentral location at a depth around 2 km. The same body was shown by MT and DG soundings as a highly resistive structure overlying a very conductive layer. Thus, we can conclude that the bottom of this lighter, resistive body is the top limit for hot fluids upward migration before lateral diffusion. Resurgence of La Starza resistive block is of course favoured by its relative lightness with respect to the surrounding rocks.

Acknowledgements

The authors wish to thank Giovanni Orsi and Andreas Tzanis, who carefully reviewed the manuscript and gave useful suggestions to improve readability. The work was performed with financial grants from the European Community (TOMAVE project) and the Italian Group of Volcanology, Department of Civil Defence.

REFERENCES

BARBERI, F., E. CASSANO, P. LA TORRE and A. SBRANA (1991): Structural evolution of Campi Flegrei caldera in light of volcanological and geophysical data, *J. Volcanol. Geotherm. Res.*, **48**, 33-49.

BERRINO, G., G. CORRADO, G. LUONGO and B. TORO (1984): Ground deformation and gravity change accompanying the 1982 Pozzuoli uplift, *Bull. Volcanol.*, **47**, 187-200.

BIANCHI, R., A. CORADINI, C. FEDERICO, G. GIBERTI, P. LANCIANO, J.P. POZZI, G. SARTORIS and R. SCANDONE (1986): Modeling of surface deformations in volcanic areas. The 1970-72 and 1982-84 crises of Campi Flegrei, Italy, *J. Geophys. Res.*, **92**, 14139-14150.

BONAFEDE, M. (1991): Hot fluid migration: an efficient source of ground deformation. Application to 1982-1984 crisis at Campi Flegrei, Italy, *J. Volcanol. Geotherm. Res.*, **48**, 187-198.

CASSANO, E. and P. LA TORRE (1987): Phlegrean Fields. Geophysics, *Quad. Ric. Sci.*, CNR, **114**, 103-131.

DI MAIO, R. and D. PATELLA (1999): Basic theory of electrokinetic effects associated with earthquakes, *Boll. Geofis. Teor. Appl.*, **33**, 145-154.

DI MAIO, R., D. PATELLA, Z. PETRILLO, A. SINISCALCHI, G. CECERE and P. DE MARTINO (2000): Application of electric and electromagnetic methods to the definition of the Campi Flegrei caldera (Italy), *Ann. Geofis.*, **43** (2), 375-390.

DI VITO, M.A., R. ISAIA, G. ORSI, J. SOUTHON, S. DE VITA, M. D'ANTONIO, L. PAPPALARDO and M. PIOCHI (1991): Volcanism and deformation since 12 000 years at Campi Flegrei caldera (Italy), *J. Volcanol. Geotherm. Res.*, **91**, 221-246.

HUNSCHE, U., A. RAPOLLA, G. MUSSMAN and L. ALFANO (1981): Application of magnetotelluric and DC electrical resistivity methods in the Neapolitan geothermal area, *J. Geophys.*, **49**, 26-34.

IULIANO, T., P. MAURIELLO and D. PATELLA (2001): Looking inside Mount Vesuvius by potential fields integrated geophysical tomographies, *J. Volcanol. Geotherm. Res.* (in press).

MAURIELLO, P. and D. PATELLA (2001a): On the localisation of maximum depth gravity anomaly sources by a distribution of equivalent point masses, *Geophysics*, **66**.

MAURIELLO, P. and D. PATELLA (2001b): Gravity probability tomography: a new tool for buried mass distribution imaging, *Geophys. Prospect.*, **49**, 1-12.

MAURIELLO, P. and D. PATELLA (2001c): Magnetic buried sources discrimination by probability tomography, *Geophys. Prospect.* (submitted).

MOGI, K. (1958): Relations of the eruptions of various volcanoes and the deformation of the ground surface around them, *Bull. Earth Res. Inst. Tokyo Univ.*, **38**, 99-134.

MONACO, F., D. PATELLA, A. RAPOLLA, N. ROBERTI and A. SINISCALCHI (1986): Prospezioni magnetotelluriche nei Campi Flegrei, *Bollettino del Gruppo Nazionale per la Vulcanologia, CNR, Roma*, 347-356.

ORSI, G., S. DE VITA and M. DI VITO (1996): The restless, resurgent Campi Flegrei nested caldera (Italy): constraints on its evolution and configuration, *J. Volcanol. Geotherm. Res.*, **74**, 179-214.

ORSI, G., C. DEL GAUDIO, S. DE VITA, S.M. PETRAZZUOLI, G. RICCIARDI and C. RICCO (1999a): Short-term ground deformation and seismicity in the nested Campi Flegrei caldera (Italy): an example of active block-resurgence in a densely populated area, *J. Volcanol. Geotherm. Res.*, **91**, 415-451.

ORSI, G., D. PATELLA, M. PIOCHI and A. TRAMACERE (1999b): Magnetic modelling of the Phlegraean Volcanic district with extension to the Ponza archipelago, Italy, *J. Volcanol. Geotherm. Res.*, **91**, 345-360.

ORSI, G., S. PETRAZZUOLI and K. WOHLETZ (1999c): The interplay of mechanical and thermo-fluid dynamical system during an unrest episode in calderas: the Campi Flegrei caldera (Italy) case, *J. Volcanol. Geotherm. Res.*, **91**, 361-380.

PATELLA, D. (1997a): Introduction to ground surface self-potential tomography, *Geophys. Prospect.*, **45**, 653-681.

PATELLA, D. (1997b): Self-potential global tomography including topographic effects, *Geophys. Prospect.*, **45**, 843-863.

ROSI, M. and A. SBRANA (1987): Phlegrean Fields. Introduction, geological setting of the area, stratigraphy, description of mapped products, petrography, tectonics, *Quad. Ric. Sci.*, CNR, **114**, 9-93.